LEDAPS surface reflectance product description
Version 2.0, January 2007

Top of the atmosphere reflectance in Red (band 3), Green (band 2), Blue (band 1) of Landsat ETM+

LEDAPS Surface reflectance in Red (band 3), Green (band 2), Blue (band 1) of Landsat ETM+

Eric Vermote
University of Maryland at College Park /Dept Geography and NASA/GSFC Code 614.5
eric@ltdri.org

and

Nazmi Saleous
United Arab Emirates University

Table of Content

1. Introduction/Rationale

Directional surface reflectance is defined as the ratio between the radiance measured in specific observation geometry (zenith and azimuth) and a direct source of illumination (zenith and azimuth) in an infinitely small solid angle. The directional surface reflectance is determined from satellite observations though the atmospheric correction process. When properly retrieved, the directional reflectance is fully decoupled from the atmospheric signal, and thus represents the value that would be measured by an ideal sensor held at the same sun-view geometry and located just above the Earth's surface if there was no atmosphere.

Directional surface reflectance is the most basic remotely sensed surface parameter in the solar reflective wavelengths. It therefore provides the primary input for essentially all higher-level surface geophysical parameters, including Vegetation Indices, Albedo, LAI/FPAR, Vegetation Indices, Burned Area, Land Cover and Land Cover Change. Directional surface reflectance is also used in various "imagery" applications to detect and monitor changes on the Earth's surface (e.g., anthropogenic impacts, red-green-blue images).

In practice, atmospheric correction is typically achieved by inverting a highly parameterized model of atmospheric radiative transfer coupled to a surface reflectance model. For speed and simplicity, the surface reflectance is often assumed to be Lambertian. As atmospheric radiative transfer modeling is relatively mature, several methods could be used to model the surface/atmosphere interaction (e.g., Successive Order of Scattering, Doubling adding, Monte Carlo simulation). The main challenge to the operational implementation of these models lies in the assignment of the atmospheric parameters and the a priori knowledge of the surface BRDF – strictly necessary for a full inversion. Approaches to operationally retrieving the atmospheric parameters have advanced considerably into the last 10 years as remote sensing instruments capable of retrieving atmospheric properties (aerosol, ozone, water vapor, etc..) have been put into operation. In the absence of operational retrievals, atmospheric climatology or forecasted values can be applied, although product accuracy degrades considerably. The determination of surface BRDF at the operational level is currently practical only for satellite sensors with single-pass multi-angular capability, such like MISR or POLDER. However, surface BRDF represents a second order effect and should introduce only a consistent bias and not influence inter-annual variability analysis.

This document presents the theoretical background and implementation of the atmospheric correction used by the Landsat Ecosystem Disturbance Adaptive Processing System (LEDAPS) project at NASA Goddard Space Flight Center (http://ledaps.nascom.nasa.gov/ledaps/ledaps_NorthAmerica.html). A preliminary version of the reflectance product (version 1) was released in April 2005 and documented in Masek et al (2006). This document (version 2, January 2007) updates that earlier version.

2. Theoretical background

The atmospheric "perturbation" of the directional surface reflectance signal depends on the type and characteristics of atmospheric particles interacting with the radiation. The gas molecules ($N_2,O_2,O_3,H_2O,CO_2,\ldots$) scatter radiation according to Rayleigh's theory (i.e., molecular scattering). Gas molecules also absorb radiation in specific spectral bands with bandwidths varying by species, and the atmospheric pressure and temperature vertical profiles. Aerosols, which are suspended particles ranging from about $10^{-3}\mu$m to about 20μm, scatter and absorb radiation according to the Mie and Geometric Optics theory. The former is used for aerosols with diameters on the order of the radiation wavelength; the latter assumes larger particles as individual spheres with given refractive real and imaginary refractive indices.

Atmospheric correction removes or reduces the effects of these atmospheric perturbations. In an idealized case of a Lambertian surface (angularly uniform reflectance) and in a narrow spectral band (here referred to with the index [i]) outside of the main absorption feature of water vapor, the top-of-atmosphere signal could be written (Vermote et al., 1997) as:

$$r_{TOA}^{i}(q_s,q_v,f,P,t_A^i,w_0^i,P_A^i,U_{H_2O},U_{O_3}) = Tg_{OG}^i(m,P)Tg_{O_3}^i(m,U_{O_3}) \begin{bmatrix} r_{atm}^i(q_s,q_v,f,P,Aer^i,U_{H_2O}) + \\ Tr_{atm}^i(q_s,q_v,P,Aer^i)\dfrac{r_s}{1-S_{atm}^i(P,Aer^i)r_s}Tg_{H_2O}^i(m,U_{U_{H_2O}}) \end{bmatrix} \quad (1)$$

Where:
ρ_{TOA} is the reflectance at the top of the atmosphere,
Tg is the gaseous transmission by water vapor, Tg_{H_2O}, by ozone, Tg_{O_3}, or other gases, Tg_{OG} (e.g. $CO_2,\ldots$)
ρ_{atm} is the atmosphere intrinsic reflectance,
Tr_{atm} is the total atmosphere transmission (downward and upward)
S_{atm} is the atmosphere spherical albedo,
ρ_S is the surface reflectance to be retrieved by the atmospheric correction procedure,

The geometrical conditions are described by θ_s, the solar zenith angle, θ_v, the view zenith angle and ϕ, the difference between the solar and view azimuth angle,

P is the pressure which influences the number of molecules in the atmosphere and the concentration of absorbing gases.

τ_A, ω_0 and P_A describe the aerosol properties and are spectrally dependent,
τ_a is the aerosol optical thickness,
ω_0 is the aerosol single scattering albedo,
P_A is the aerosol phase function,
U_{H_2O} is the integrated water vapor content ,
U_{O_3} is the integrated ozone content ,
m, is the air-mass computed as $1/\cos(\theta_s)+1/\cos(\theta_v)$

The effect of the water vapor on the atmosphere intrinsic reflectance can be approximated as:

$$r^i_{atm}(q_s,q_v,f,P,Aer^i,U_{H_2O}) = r^i_R(q_s,q_v,f,P) +$$

$$\left(r^i_{R+Aer}(q_s,q_v,f,P,Aer^i) - r^i_R(q_s,q_v,f,P)\right)Tg^i_{H_2O}(m,\frac{U_{U_{H_2O}}}{2})$$

(2)

where ρ_R represent the reflectance of the atmosphere due to molecular (Rayleigh) scattering, and ρ_{R+Aer} represents the reflectance of the mixing molecules and aerosols. Accounting correctly for the mixing and the so-called coupling effect (Deschamps et al.,1983) is important for achieving high accuracy in the modeling of atmospheric effect. This approximation conserves the correct computation of the coupling, and supposes that the water vapor is mixed with aerosol and that the molecular scattering is not affected by the water vapor absorption.

3. Practical Implementation

The transmission, intrinsic reflectance, and spherical albedo terms are computed using the Vectorial version of the 6S radiative transfer code (Kotchenova et al., 2006). Since the cost of running 6S for each pixel will be prohibitive, 6S is run early on in the process to generate a look up table (LUT) accounting for pressure, water vapor, ozone and geometrical conditions over the whole scene for a range of aerosol optical thickness. The LUT is created for every TM bands and is used both in the aerosol retrieval process as well as in the correction step at the end. Figure 1 summarizes the different step of the algorithm.

Ozone concentrations are derived from Total Ozone Mapping Spectrometer (TOMS) data aboard the Nimbus-7, Meteor-3, and Earth Probe platforms. The gridded TOMS ozone products are available at a resolution of 1.25 longitude and 1.00 latitude from the NASA GSFC Data Active Archive Center (DAAC). In cases where TOMS data are not available (e.g., 1994–1996), NOAA's Tiros Operational Vertical Sounder (TOVS) ozone data are used.

 Column water vapor is taken from NOAA National Centers for Environmental Prediction (NCEP) reanalysis data available at a resolution of 2.5 by 2.5 degrees (http://dss.ucar.edu/datasets/ds090.0/). Digital topography (1 km GTopo30) and NCEP surface pressure data are used to adjust
Rayleigh scattering to local conditions.

Like other atmospheric correction schemes for MODIS and Landast, we make use of the dark, dense vegetation (DDV) method of Kaufman et al. (Kaufman et al., 1997; Remer et al., 2005) in order to extract aerosol optical thickness (AOT) directly from the imagery. Based on the physical correlation between chlorophyll absorption and bound water absorption, this method postulates a linear relation between shortwave-infrared (2.2 µm)

surface reflectance (nearly unaffected by the atmosphere) and surface reflectance in the visible bands. By using the relation to calculate surface reflectance for the visible bands, and comparing the result to the TOA reflectance, aerosol optical depth may be estimated. For LEDAPS AOT estimation, each image is averaged to 1 km resolution (to suppress local heterogeneity), and candidate "dark targets" with TOA are selected. For these targets, we assume a correlation only between the blue (0.45–0.52) and SWIR (2.2µm) bands, such that . Water targets are excluded. The specific relation is derived from an analysis of data from Aerosol Robotic Network (AERONET) sites where AOT is measured directly (Figure 2). The calculated AOT in the blue wavelengths is propagated across the spectrum using a continental aerosol model. A sanity check for the aerosol is performed by analyzing the surface reflectance derived in the red for each 30m pixels contained in the 1km grid cell, if too many "unphysical" values are found, the aerosol retrieval at this 1km location is rejected. The valid aerosol optical thicknesses at 1km are interpolated spatially between the dark targets using a spline algorithm. The interpolated AOT, ozone, atmospheric pressure, and water vapor are supplied to the 6S radiative transfer algorithm, which then inverts TOA reflectance for surface reflectance for each 30-m pixel.

As noted above, water targets are excluded from the aerosol retrieval. However, interpolation of valid (ie. land) aerosol targets occurs across the entire scene. Thus, the surface reflectance of small lakes surrounded by land is likely to be reasonable, while the reflectance of open ocean water (far from any valid aerosol target) is likely to be problematic.
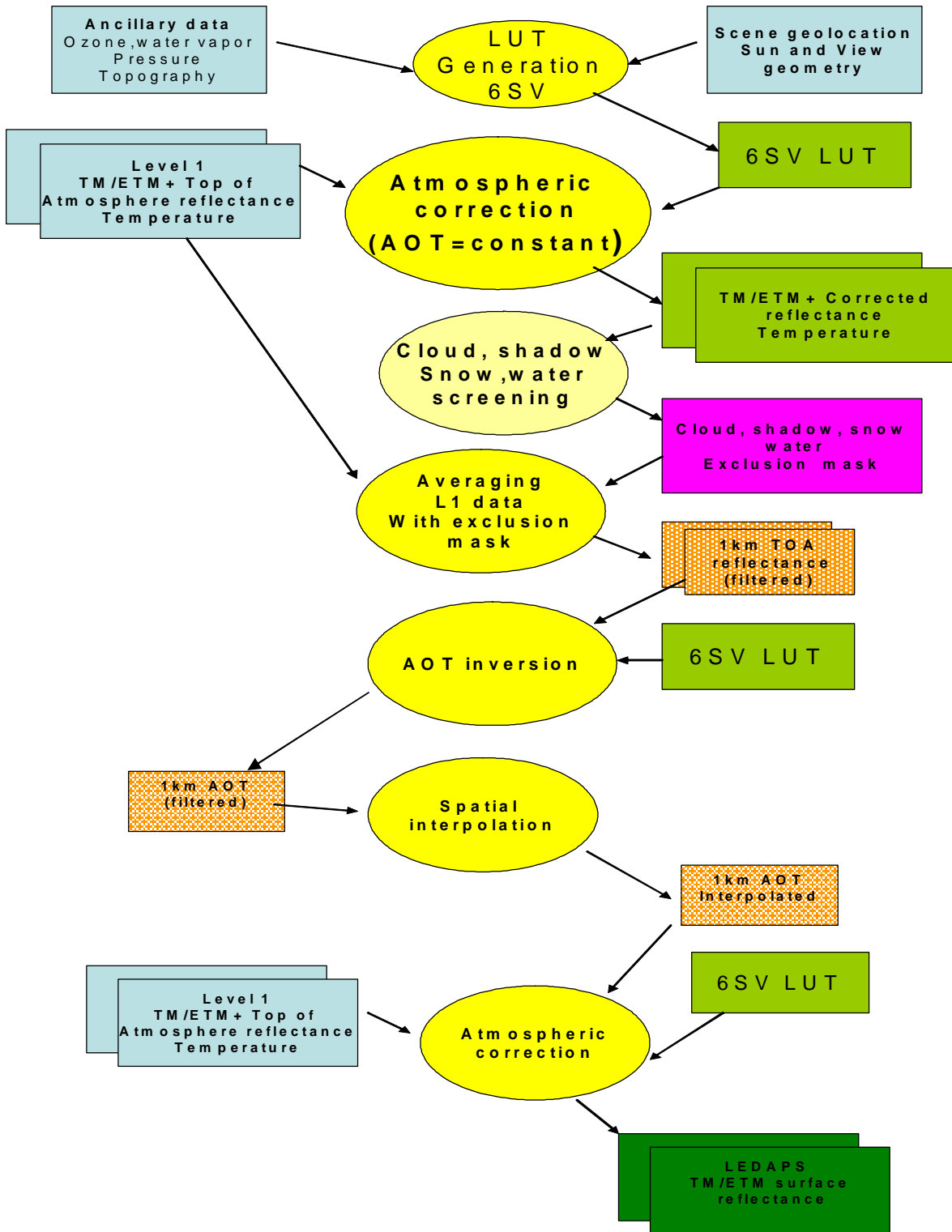
Figure 1: Atmospheric correction processing flowchart.
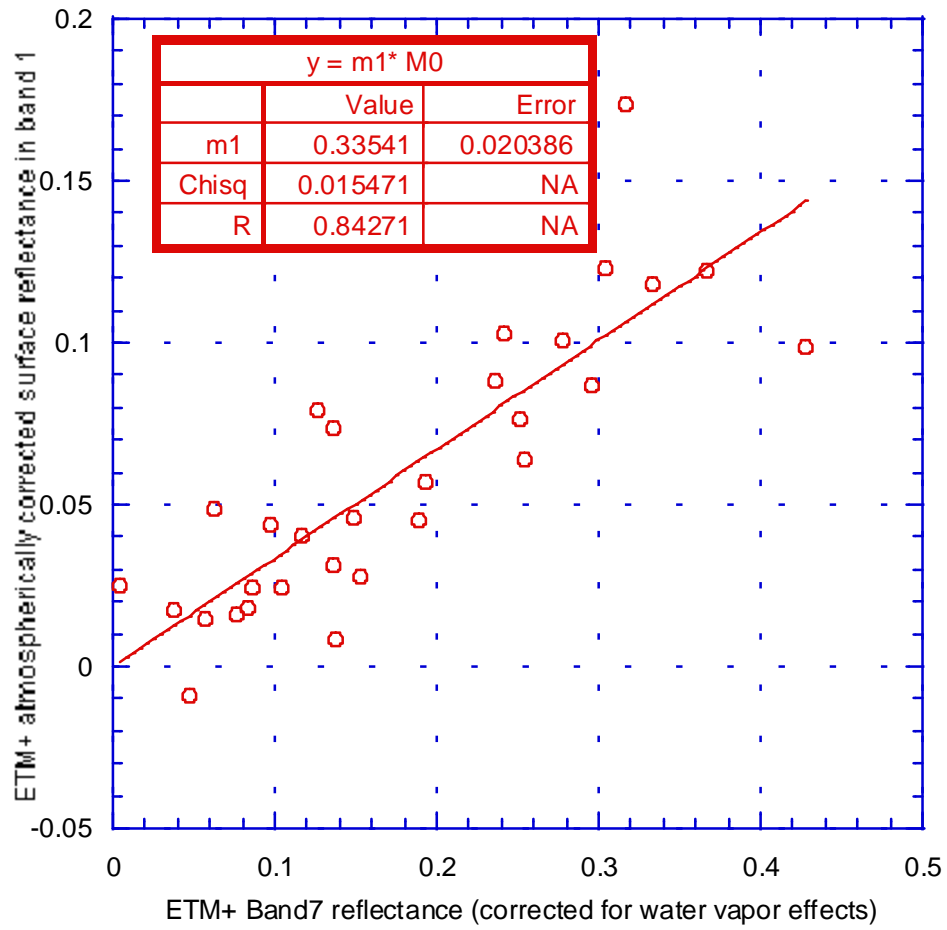
Figure.2: Relation between the ETM+ blue and SWIR reflectances.

4. Exclusion Mask (water, cloud, shadow, snow)

Prior to application of the cloud screening, the reflectance data are corrected for very clear atmosphere conditions (aerosol optical thickness =0.01).

4.1 Water Test

First, the water pixels are discarded from the analysis. The water test uses several aspect of the reflectance spectrum of the water to makes its determination: The low signal observed over clear water particularly in the near infrared and beyond (band 4 and band 5) and the possible abnormal NDVI values (land surface have a NDVI above 0.10).

The pixel is declared water if the water test (WT) is true:

WT=(NDVI < 0.1) OR (r(band 4) < 0.04 AND r(band 5) < 0.05))

4.2 Cloud Mask Test (First Pass)

The cloud mask makes use of four different criteria to identify clouds.

1) The whiteness of the cloud in the visible, in particular across the blue and the red. This test is called the Visible Reflectance anomaly threshold VRA. Note that this test may confuse clouds and high aerosol concentration. The VRA test (VRAT) successfully concludes to the presence of clouds if,

VRAT= (r^s(blue=band1)-0.5.r^s(Red=band3)) > 0.08

2) The fact that the clouds are colder than the underlying surface (because at a higher altitude), this test can fails for cold surface (snow), or even dense forest which appears to have similar temperature than low altitude clouds. An other problem is the temperature of the colder surface is not directly available, so we use in a first pass the temperature of the air at 2m from the NCEP data. Other problems may include the atmospheric effect on brightness temperature derived from band 6 used in this test.
The brightness temperature test (BTT) for cloud is positive if:

BTT=Brightness Temperature (Band 6) < Air temp(NCEP)-20 [Degree Celsius]

3) This next test is a heritage from different cloud masks in particular CLAVR. It is a pure reflective test based on the fact the clouds have higher reflectance

than clear pixels. It is performs using the red and near infrared, the test is positive for clouds if:

$$RT = r^s(band\ 3) > 0.4\ or\ r^s(band\ 4) > 0.6$$

4) The last test is also an heritage test that also used the principle that the NDVI of land surface is bounded between 0.1 for desert surface to much higher values for different type of vegetation cover (typically up to 0.8). NDVI below 0.1 are usually associated with clouds. In this particular form, the simple ratio in use in lieu of the NDVI but the principle is the same. The spectral ratio test (SRT) is positive for clouds if:

$$SRT = 0.9 < (r^s(band\ 4)\ /r^s(\ band\ 3)) < 1.3$$

In the first pass, the goal is to identify pixels that are without a doubt clear, in order to compile statistics that will be used to refine the air temperature at 2 meters obtained from NCEP. The NCEP air temperature at 2m does not have the necessary spatial and temporal resolution for accurate cloud screening.

The pixels are declared clear in the first pass if they are not tested as water pixel, and they did not meet any of the criteria outlined in 1-4 (SRT, RT, BTT, BTT or VRAT). *Another test is also added to reject any possible unfiltered water pixel or pixel contaminated by shadow, it uses the band 7 reflectance and requires that the selected pixels have a reflectance > 0.03.*

The statistics record the mean and standard deviation temperature of the clear pixels in one kilometer grid that contains in addition the mean and standard deviation of the reflectance in band 7.

4.3 Cloud Mask Test (Second Pass)

In the second pass the temperature of the clear pixels of the first pass, is used to refine the air temperature at 1km resolution. If no statistics at one kilometer are available the default temperature used in step one is still used (NCEP), if results are available both the mean temperature and standard deviation are used. A pixel is declared as cloudy in the second pass if:

The reflectance in band 7 is greater than 0.03 AND
a) The brightness temperature of this pixel is lower than the final air temperature threshold
OR
b) If it is brightness temperature is lower than the air temperature threshold by no more than 4 degree C, but it VRAT is positive for clouds

4.4 Snow Test (Second Pass)

The snow test is only done in the second pass. It uses the standard NDSI threshold (0.3) used in the MODIS algorithm (expect in that case, we use corrected reflectance and not top of the atmosphere), a temperature test (which was also adopted in the collection 5 MODIS algorithm) and a reflective test to prevent false detection.

A pixel is defined as snow if:

$NDSI=(r^s(band2)-r^s(band5))/ (r^s(band2)+r^s(band5)) > 0.3$
AND
Brigthness Temperature > 280 Kelvin
AND
$r^s(band4) > 0.2$

4.4 Cloud shadow screening

The algorithm for cloud shadow uses a geometric determination of the shadow based on the cloud mask and the estimated altitude of cloud derived from the brightness temperature in band 6. From the refined air temperature at 2m obtained from the statistics compiled in the first pass of the cloud mask, the altitude of the cloud in kilometer is approximated by:

Cloud Altitude = (air temperature-Brighthness Temperature (band6))/ **CF**

All the temperature being expressed in Kelvin

CF (the conversion factor) ranges from 1 to 6 allowing the algorithm to generate several possible altitudes for the clouds. From that range of altitudes, a range of shadow is cast on the image using the sun view and azimuth angle.

5. Validation

Three approaches are being used to validate Landsat surface reflectance (SR) products:
1. comparison with near-simultaneous (15 minutes apart) MODIS 500m single-swath surface reflectance data.
2. comparison of Landsat aerosol optical thickness with that obtained by simultaneous AERONET sun photometer network observations.
3. Evaluation of the LEDAPS Surface Reflectance product by comparison to a reference surface reflectance data obtained using the 6SV radiative transfer code and the AERONET data as input to the radiative transfer code.

5.1. Comparison with Aeronet Aerosol Optical Thickness

Aerosol Robotic Network (AERONET) sites record aerosol properties throughout the world, and several of these records extend back to the early 1990's (Holben et al., 1998). The LEDAPS dataset includes several AERONET sites, and observations from 21 of these sites were compared with simultaneous aerosol optical thickness obtained using the image-based approach discussed above (Table 1, Figure. 3).

All AOT values reported are for the blue wavelengths. Results suggest reasonable agreement with AERONET observations. Spatial patterns for the sites suggest that land cover type may influence the aerosol retrievals (Figure 4), although this effect is probably not as strong as the surface reflectance product.

For comparison, uncertainties in MODIS land AOT retrievals is (0.05 + 0.2*AOT), which have also been plotted on Figure. 3.

AERONET Site	TM Scene	Date	AOT blue Aeronet	AOT blue ETM
Howland	p011r029	2002253	0.4	0.1767
GSFC	p015r033	2001278	0.25	0.257
MD_Science_Center	p015r033	2001278	0.29	0.414
SERC	p015r033	2001278	0.25	0.294
BSRN_BAO_Boulder	p033r032	2000261	0.05	0.024
Sevilleta	p034r036	2000130	0.12	0.135
Bratts_Lake	p035r025	2000208	0.2	0.161
Bratts_Lake	p036r025	2001217	0.08	0.026
Maricopa	p036r037	2000167	0.09	0.1889
Tucson	p036r037	2000167	0.11	0.056
UCLA	p041r036	2000122	0.2	0.275
Shirahama	p109r037	2001105	0.3	0.344
Anmyon	p116r035	2001266	0.11	0.156
Moscow_MSU_MO	p179r021	2002150	0.17	0.059
Rome_Tor_Vergata	p191r031	2001215	0.49	0.384
Ilorin	p191r054	2000037	1.05	0.921
Ouagadougou	p195r051	2001195	0.275	0.346
Lille	p199r025	2000237	0.29	0.38
Palaiseau	p199r026	2000237	0.22	0.156
Thompson	p033r021	2001260	0.06	0.033
HJAndrews	p045r029	1999275	0.08	0.033

Table 1: AERONET and ETM+ AOT comparisons
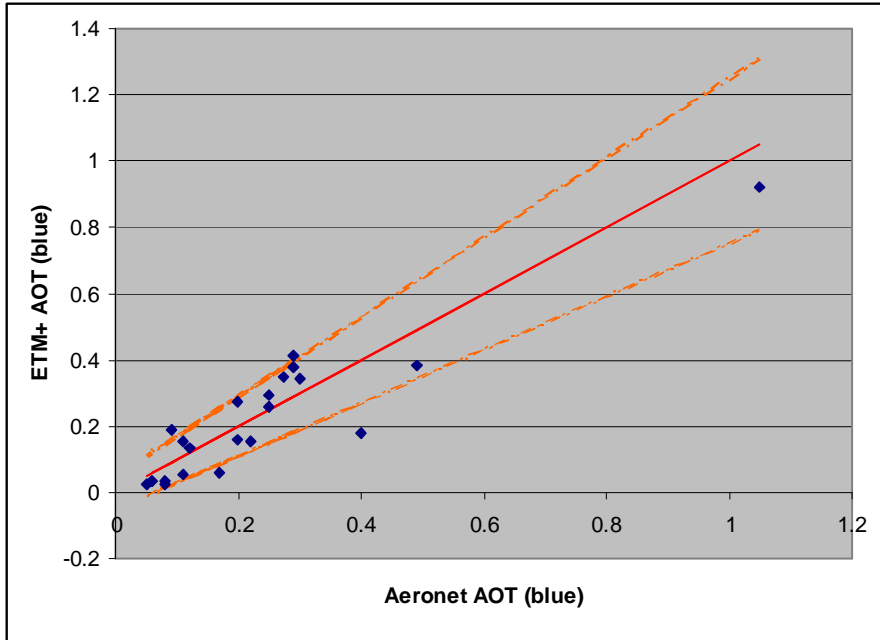
Figure. 3: ETM+ AOT values regressed against simultaneous AERONET AOT values for the blue band. Solid red line is the one-to-one line, dashed lines represent MODIS AOT uncertainties of (0.05+0.2*AOT).
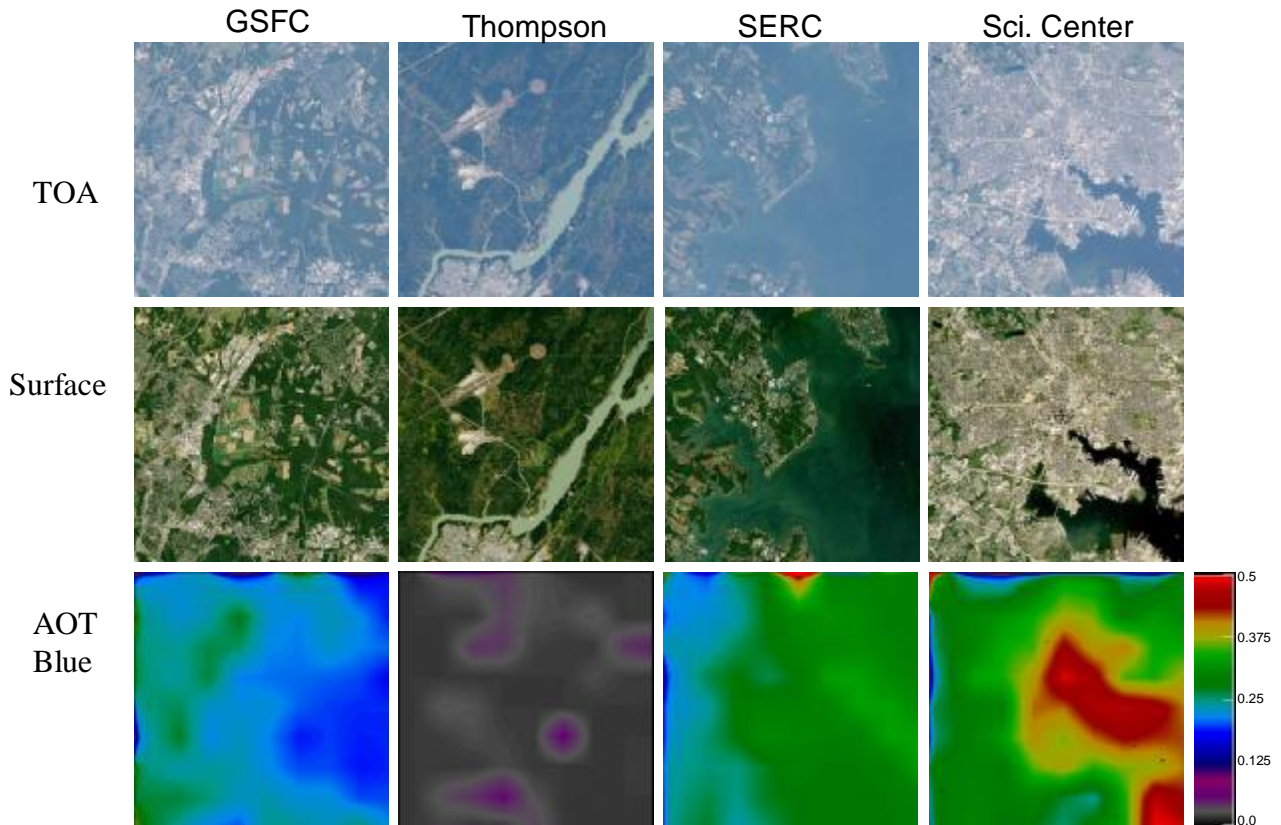
Figure 4: TOA reflectance, atmospherically corrected surface reflectance, and AOT (blue wavelengths) for the AERONET sites used in the study.

5.2. Comparisons with MODIS

MODIS 500m Surface Reflectance (SR) products were processed from individual swaths, and registered with Landsat-7 ETM+ SR products from images acquired within 15 minutes. The Landsat SR products were aggregated to 500m resolution by averaging blocks of pixels. For one scene in Canada (BOREAS study region), three sub-windows from each dataset were extracted and compared (Figure 5).

Plotting histograms before and after correction for each sub-window suggests that, for most spectral bands, differences between MODIS and ETM+ SR values are negligible (Figures. 6,7,8). One exception is the blue band, where ETM+ SR values trend ~1% higher than the comparable MODIS band.

For two sub-windows, some differences also exist for the shortwave infrared (1.6μm) band, although the spread of the data distribution makes it difficult to detect a consistent trend.
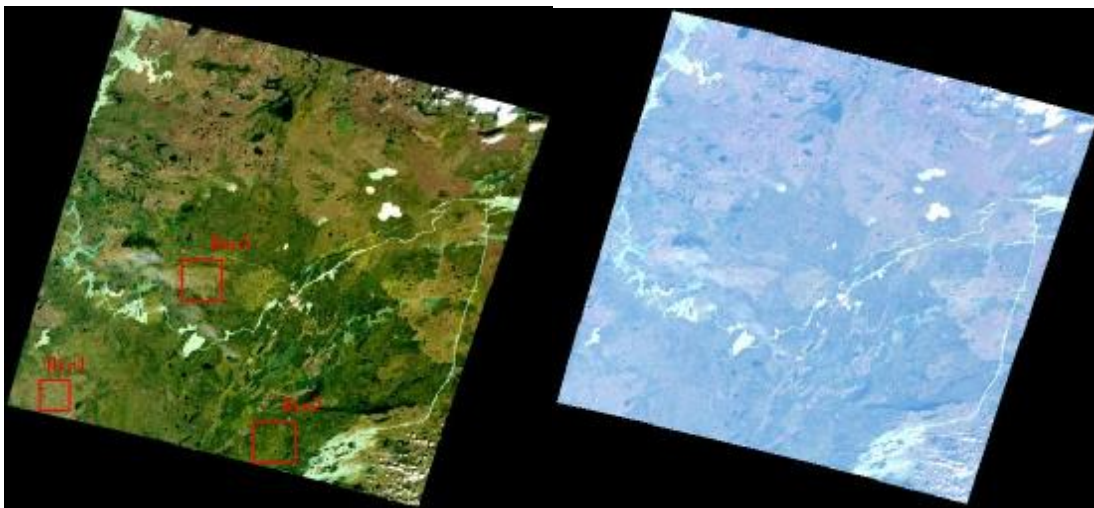
Figure 5: BOREAS ETM+ scene, Surface reflectance (Left) and top-of-atmosphere (right) with locations of sub-windows for comparison with MODIS surface reflectance (Scene: p033r021,Date: 09/17/2001)
.
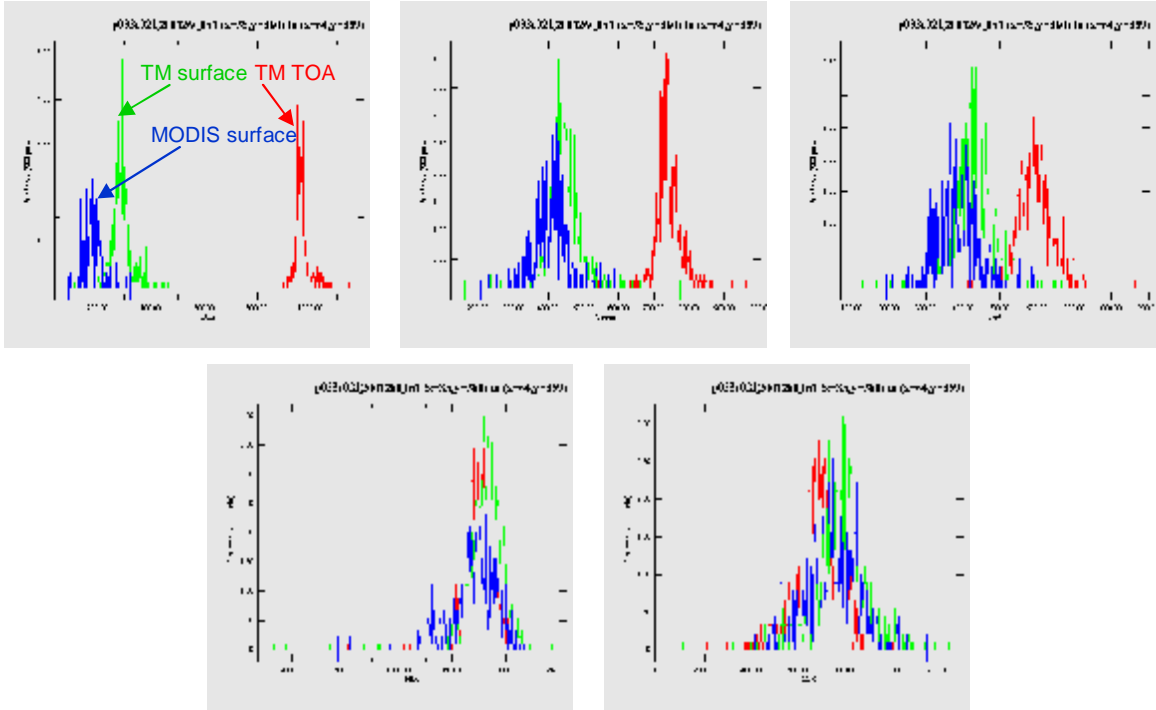
Figure 6: Histograms of Landsat TOA reflectance (red), MODIS surface reflectance (blue) and Landsat surface reflectance (green) for the following bands: blue (upper-left), green (upper-center), red (upper-right), near-infrared (lower-left), mid-infrared (lower-right)
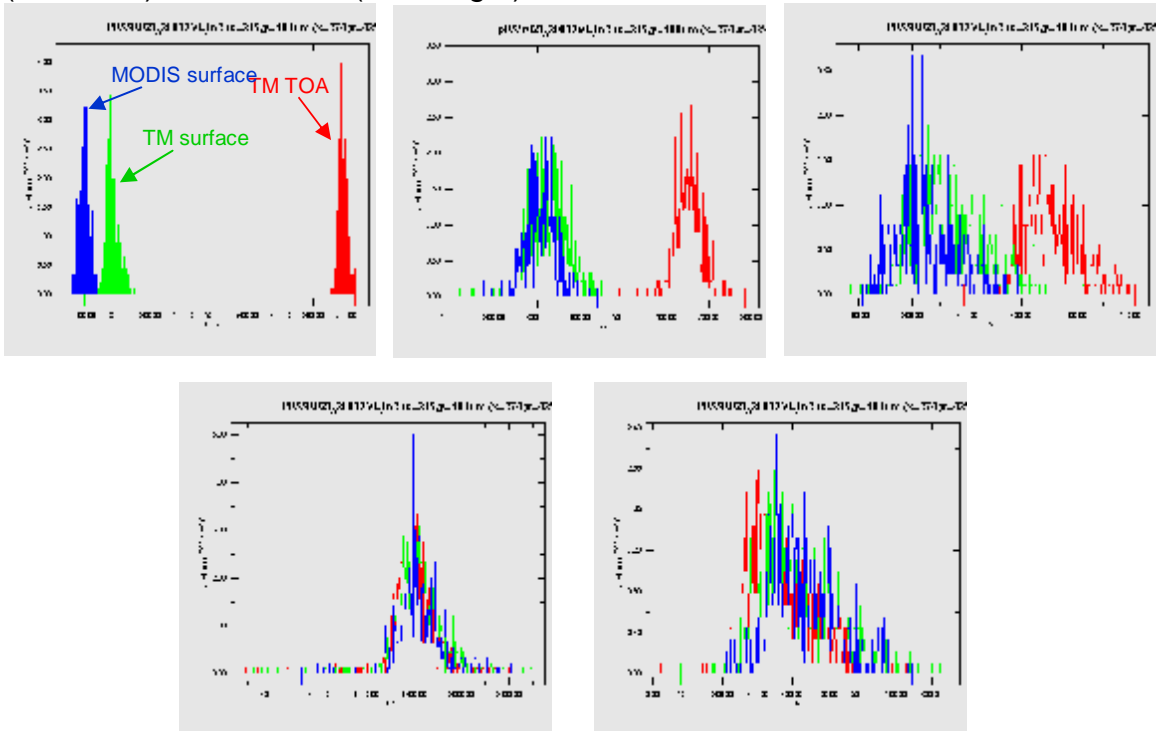
Figure 7: Same as Figure 6 but for Subwindow 2
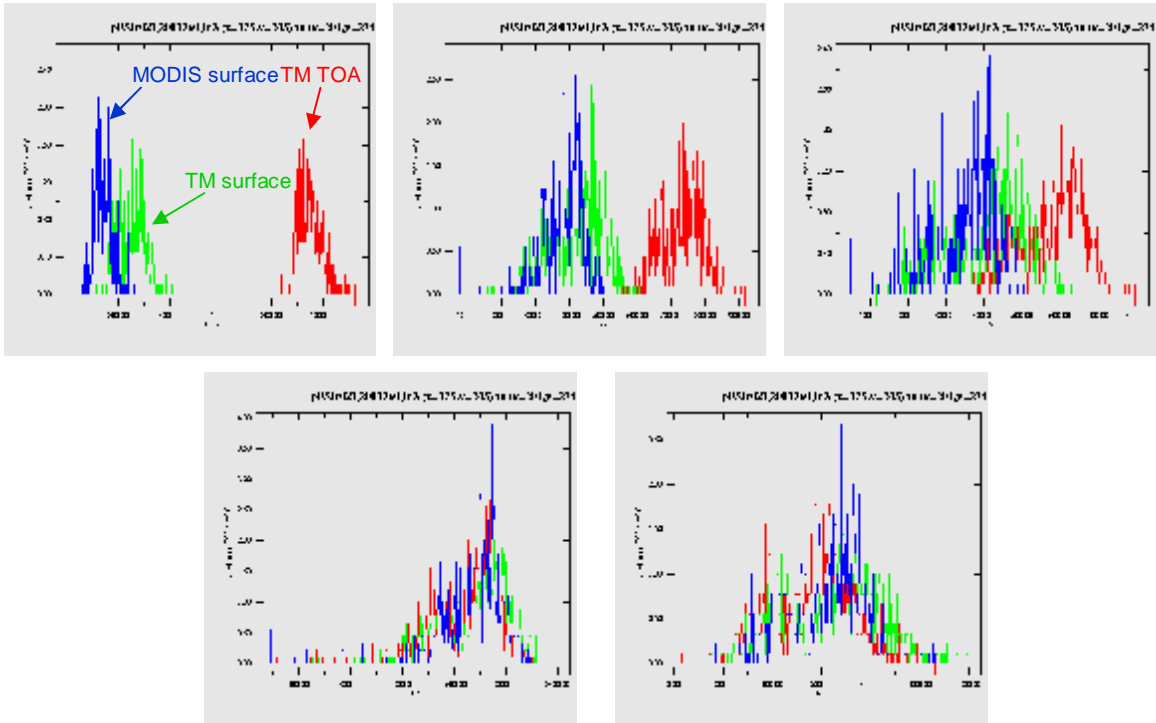
Figure 8: Same as Figure 6 but for Subwindow 3

5.3. Evaluation of the surface reflectance product over the AERONET sites.

A preliminary subset of LEDAPS scenes has been analyzed to establish quantitatively the performance of the surface reflectance product. The approach is following the analysis put in place for the evaluation of the MODIS collection 5 reflectance product. For a subset of 200 by 200 pixels around the AERONET sites, Aerosol Optical Thickness (AOT), aerosol model and column water vapor derived from AERONET measurements were used in 6S to perform atmospheric correction of Level 1 Top Of Atmosphere reflectance from ETM+ and provide a reference used in assessing the performance of the LEDAPS surface reflectance product. A preliminary data set of is presented in Table 2

The performance of the LEDAPS surface reflectance product was evaluated for band 3 (Figure 8a), band 4 (Figure 8b) and the NDVI \(Figure 8c) computed from band 3 and band 4.

DATE.PATH/ROW	Aerosol Optical Thickness	Aeronet Site
2000122.w2p041r036	0.0932345	Rogers_Dry_Lake
2000122.w2p041r037	0.162749	UCLA
2000170.w2p009r029	0.0449007	Kejimkujik
2000191.w2p028r035	0.0858729	Cart_Site
2000247.w2p036r038	0.0365191	Tucson
2000261.w2p022r039	0.0722956	Stennis
2000267.w2p048r026	0.0727889	Saturn_Island
2001155.w2p034r036	0.105914	Sevilleta
2001216.w2p029r030	0.133025	Sioux_Falls
2001217.w2p036r025	0.0797376	Bratts_Lake
2001218.w2p043r028	0.0735507	Rimrock
2001267.w2p034r032	0.0717833	BSRN_BAO_Boulder
2001278.w2p015r033	0.147011	GSFC

Table 2: List of scenes used in the evaluation of the LEDAPS surface reflectance product.
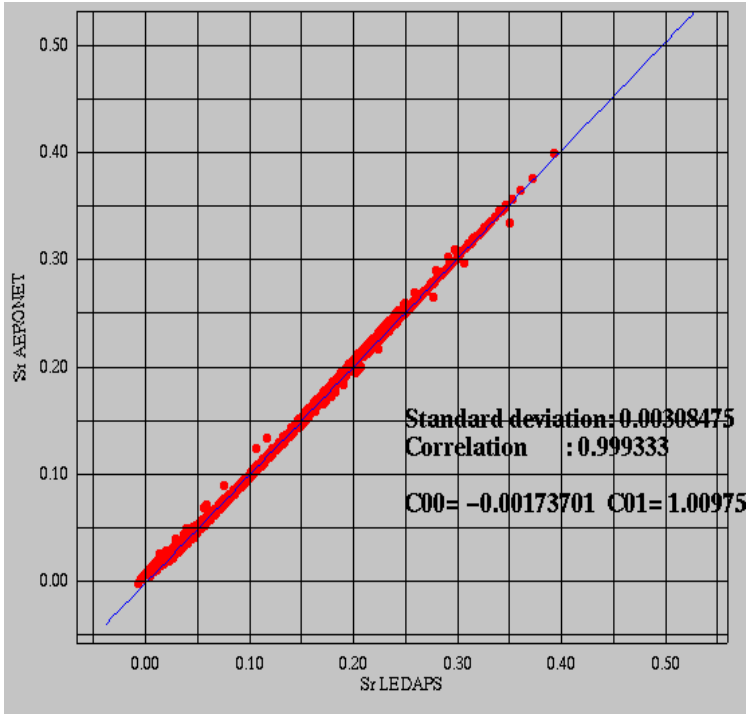
Figure 8a: Comparison of the reference reflectance derived from 6S and AERONET data with the LEDAPS surface reflectance product in band 3.
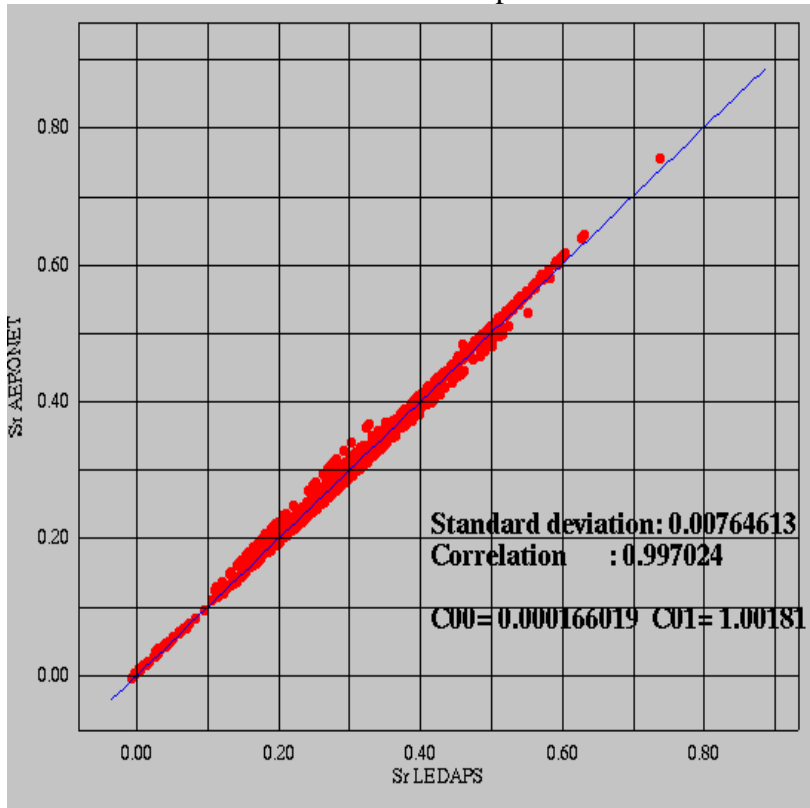
Figure 8b: Comparison of the reference reflectance derived from 6S and AERONET data with the LEDAPS surface reflectance product in band 4.
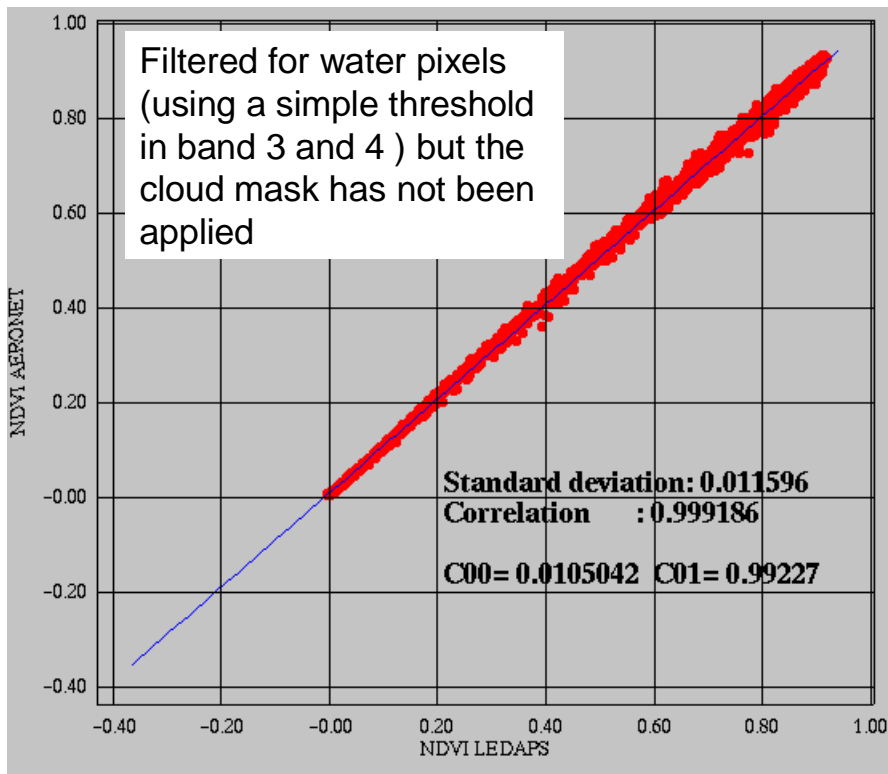
Figure 8c: Comparison of the reference NDVI derived from 6S and AERONET data with the LEDAPS NDVI product.

.

6. Known Issues

Known issues emerging from our analyses (to be corrected in future releases) include:

1. Cloud/Cloud Shadow/snow mask is prone to errors - this part of the algorithm needs to be refined and updated.
2. The aerosol retrieval over water needs to be implemented for coastal studies
3. A geographic/seasonal refinement of the aerosol model could be implemented, we have use so far a continental aerosol model. This aerosol model is probably well adapted for Northern America but may not be appropriate globally (e.g South Africa where biomass burning aerosol dominates).
4. Atmospheric point spread function should be implemented because this effect is important for 30m pixels.

7. References

Deschamps, P.Y., Herman, M. and Tanre, D. (1983). Modeling of the atmospheric effects and its applications to the remote sensing of ocean color. *Appl. Optics.,* **22:** 3751-3758.

Holben B.N., Eck T.F., Slutsker I., Tanré D., Buis J.P., Setzer A., Vermote E.F., Reagan J.A., Kaufman Y.J., Nakajima T., Lavenue F., Jankowiak I., Smirnov A., 1998, AERONET - A federated instrument network and data archive for aerosol characterization, Remote Sensing of the Environment, 66:(1) 1-16.

S. Y. Kotchenova, E. F. Vermote, R. Matarrese, & F. Klemm, 2006 Validation of a new vector version of the 6S radiative transfer code for atmospheric correction of MODIS data: Part I – Path Radiance, Applied Optics, Vol 45., No. 26, 6762-6774..

Kaufman, Y.J., Wald, A.E., Remer, L.A. et al., 1997, The MODIS 2.1-micron channel Œ correlation with visible reflectance for use in remote sensing of aerosol, IEEE Trans. Geosci. Remote Sens., 35, 1286-1296.

Masek, J.G., E.F. Vermote, N. Saleous, R. Wolfe, F.G. Hall, F. Huemmrich, F. Gao, J. Kutler, and T.K. Lim, A Landsat surface reflectance data set for North America, 1990-2000, Geoscience and Remote Sensing Letters, 3, 68-72, 2006.

Remer L.A., Kaufman Y.J., Tanré D., Mattoo S., Chu D.A., Martins J.V., Li R-R., Ichoku C, Levy R. C., Kleidman R.G., Eck T.F., Vermote E., and B.N. Holben, 2005, "The MODIS Aerosol Algorithm, Products and Validation", Journal of Atmospheric Sciences, 62 (4),947-973.

Vermote E.F., Tanré D., Deuzé J.L., Herman M., Morcrette J.J., 1997, Second Simulation of the Satellite Signal in the Solar Spectrum: an overview, *IEEE Transactions on Geoscience and Remote Sensing*, 35,3,675-686.